


Structural properties of local integrals of motion across the many-body localization transition via a fast and efficient method for their construction

Safa Adami, Mohsen Amini ^{*}, and Morteza Soltani*Department of Physics, Faculty of Physics, University of Isfahan, Isfahan 81746-73441, Iran*

(Received 24 April 2022; revised 17 June 2022; accepted 1 August 2022; published 9 August 2022)

Many-body localization (MBL) is a novel prototype of ergodicity breaking due to the emergence of local integrals of motion (LIOMs) in a disordered interacting quantum system. To better understand the role played by the existence of such LIOMs, we explore and study some of their structural properties across the MBL transition. We first consider a one-dimensional XXZ spin chain in a disordered magnetic field and introduce and implement a nonperturbative, fast, and accurate method of constructing LIOMs. In contrast to already existing methods, our scheme allows obtaining LIOMs not only in the deep MBL phase but, rather, near the transition point too. Then, we take the matrix representation of LIOM operators as an adjacency matrix of a directed graph whose elements describe the connectivity of ordered eigenbasis in the Hilbert space. Our cluster-size analysis for this graph shows that the MBL transition coincides with a percolation transition in the Hilbert space. By performing finite-size scaling, we compare the critical disorder and correlation exponent ν both in the presence and absence of interactions. Finally, we also discuss how the distribution of diagonal elements of LIOM operators in a typical cluster signals the transition.

DOI: [10.1103/PhysRevB.106.054202](https://doi.org/10.1103/PhysRevB.106.054202)

I. INTRODUCTION

Currently, there is great scientific interest to gain deeper insight into the localization phenomena in many-body quantum systems. By now, it has been found that, in one dimension, an isolated interacting system of fermions that is subject to quenched disorder can undergo a phase transition from a thermal regime where transport is diffusive or subdiffusive [1–6] to the many-body localization (MBL) phase where the transport coefficients are exponentially small in the system size [7–10] and memory of the initial state is retained to arbitrarily long times [11].

It is thought that the MBL phase of such systems can be described in terms of emergent local integrals of motion (LIOMs) which form a complete set of quasilocal conserved quantities [12–14]. In the absence of interaction, such a system exhibits Anderson localization [15] for an arbitrarily small amount of disorder. The corresponding single-particle wave functions are exponentially localized in real space over a characteristic length scale which is called localization length. In this case, a complete set of LIOMs can be identified by the occupancies of these single-particle orbitals [12]. Upon turning the interaction on, multiparticle resonances start to proliferate and, hence, stronger disorder is needed to keep the system localized [7]. However, if the disorder strength is sufficiently larger than the interaction strength, the system remains in the MBL phase and LIOMs can be understood as weakly dressed single-particle orbitals [12,16].

In general, the number of ways in which a set of LIOMs can be arranged is very large and, therefore, the calculation

of all LIOMs is a complicated task practically. It was first pointed out that a complete set of LIOMs for a finite-size system can be obtained via labeling the eigenstates of the system by their corresponding LIOM eigenvalues uniquely [13,14]. Then, it was suggested to construct LIOMs (which do not form a complete basis) by computing an infinite-time average of initially local operators [17,18]. In this regard, various approaches like using Monte Carlo stochastic method [19], exact diagonalization techniques [20–23], and tensor networks [24–27] have been developed.

Although the above-mentioned construction algorithms for LIOMs have made great progress, developing and implementing a simple method that allows constructing a complete set of LIOMs with the following properties simultaneously is of major interest. A method that (i) is nonperturbative and provides quasilocal LIOMs that commute strictly with the Hamiltonian, (ii) not essentially requires strong disorder intensity, and (iii) costs much less computationally but yet has enough accuracy. In particular, the second property makes it possible to move away from the deep MBL phase toward the transition point and study some aspects of the phase transition using LIOMs. This is an interesting issue because even in the ergodic phase it is possible to define integrals of motion that are not local quantities. By increasing the strength of the disorder, one arrives in the MBL phase in which the system fails to thermalize and constants of motion are localized. Therefore, it is the structural properties of the LIOMs that directly affect the thermalization of the system [28]. So, it is always interesting to characterize the MBL transition via the properties of the LIOMs across the transition. Thus, the main objective of the following paper is twofold. First, we present an efficient scheme for computing a complete set of LIOMs in a nonperturbative manner and, second, capture certain aspects of the MBL transition by

*msn.amini@sci.ui.ac.ir

considering the resulting LIOM operators as an adjacency matrix of a graph that represents the connectivity of the eigenbasis in the Hilbert-space and undergoes a percolationlike transition.

In this paper, we describe and develop a fast method to construct a complete set of LIOMs explicitly for the random-field XXZ spin chain that can be used to study some structural properties of LIOMs near the MBL to ergodic transition. We perform our algorithm via arranging an optimized set of the eigenstates of the system in a quasilocal unitary operator which maps the physical spin operators onto effective spins operators. Such an ordered set of the eigenbasis can be obtained by assigning an integer index number to each eigenstate which determines its order in our desired set. We recognize this index number by locating the original basis vector of the Hilbert space on which that eigenstate has the largest absolute amplitude among all the eigenstates of the system. Then, in the next step, we consider the resulting LIOM operator as an adjacency matrix of a network whose elements indicate the connectivity of the eigenbasis in the Hilbert space. We illustrate that this network undergoes a percolationlike transition on crossing the transition from MBL into the ergodic phase. The percolation transition can be understood within the Hilbert-space cluster size analysis of the fragmentation of the network associated with LIOMs. Such a classical percolation analogy for the MBL transition was previously observed either by considering the Hamiltonian as a tight-binding model in Fock space [29,30] or by retaining only resonant contributions and mapping the quantum problem to rate equations [31]. However, in this paper, we underline the importance of such a transition in a network associated with LIOMs which is a key concept in MBL transition. We further provide an analysis of how local observables on the clusters of this network can quantitatively capture the ergodic to MBL transition.

The rest of the paper is organized as follows. In Sec. II, we describe our spin-1/2 model employed and introduce our algorithm to construct LIOM operators. Section III contains numerical results obtained by the implementation of our algorithm. We first represent the results concerning the locality of obtained LIOM operators. We then use the LIOM operators and show that the ergodic to MBL transition coincides with a percolation transition in a graph of eigenvectors in the Hilbert space whose structure is described by the matrix representation of LIOMs. To illustrate how the transition takes place, we perform cluster size analysis and apply finite-size scaling to compare the percolation threshold and correlation exponent ν in the presence and absence of interaction. We further discuss how the distribution of local magnetization of clusters may signals the transition and, finally, concluding remarks are given in Sec. IV.

II. MODEL AND APPROACH

A. Model Hamiltonian

We consider a standard model of MBL which is a spin-1/2 chain of length L in a random magnetic field in the z direction and can be written as

$$H = \sum_{i=1}^{L-1} J \left(\sigma_i^+ \sigma_{i+1}^- + \sigma_i^- \sigma_{i+1}^+ + \frac{1}{2} \Delta \sigma_i^z \sigma_{i+1}^z \right) + h_i \sigma_i^z, \quad (1)$$

where $\sigma_i^\pm = \sigma_i^x \pm i\sigma_i^y$ are the raising and lowering spin-1/2 operators and $\sigma_i^{x,y,z}$ denote the Pauli operators acting on spin i . Here, we use open boundary conditions and fix the exchange interaction coupling at $J = 1$. The values h_i are, also, drawn independently from a random uniform distribution $[-W, W]$ and the parameter Δ determines the anisotropy of the model. This model is known to undergo a phase transition at a critical disorder strength $W = W_c = 3.5 \pm 0.5$ from an ergodic phase to an MBL phase which depends on energy density [32,33]. In the current paper, we focus on the MBL side of the transition, $W > W_c$, in which the existence of LIOMs prevents thermalization. Using the Jordan-Wigner transformation [34], this model can be mapped to a model of spinless fermions and we are interested in two different cases when $\Delta = 0$ and $\Delta = 1$, which corresponds to the noninteracting Anderson model and an interacting and disordered fermionic model, respectively.

B. Approach

To begin, let us review the basic idea behind the LIOM scheme. We first consider a noninteracting system in which $\Delta = 0$. Upon diagonalization of the Hamiltonian in Eq. (1), one obtains a set of energy eigenvalues that uniquely identifies the system's eigenstates. In this system, which is equivalent to a single-particle Anderson model, eigenstates are exponentially localized around some localization center and their occupation numbers are mutually commuting, conserved quantities, and hence can form a complete set of LIOMs. These are the number operators,

$$n_\alpha = \sum_{ij} \psi_\alpha^*(i) \psi_\alpha(j) c_i^\dagger c_j, \quad (2)$$

in terms of which the Hamiltonian can be rewritten as

$$H = \sum_{\alpha} 2\varepsilon_{\alpha} n_{\alpha} - \sum_{\alpha} \varepsilon_{\alpha}, \quad (3)$$

where the last term on the right-hand side is the vacuum constant energy shift. It is now straightforward to define the corresponding LIOM operators in terms of the original spin operators via the Jordan-Wigner string operator as

$$\tau_{\alpha}^z = 2 \sum_{ij} \psi_{\alpha}^*(i) \psi_{\alpha}(j) \sigma_i^+ \left(\prod_{k=\min(i,j)}^{\max(i,j)} \sigma_k^z \right) \sigma_j^- - 1, \quad (4)$$

which allows us to write the Hamiltonian as

$$H = \sum_{\alpha} \varepsilon_{\alpha} \tau_{\alpha}^z. \quad (5)$$

Given the locality of the τ_{α} , one could as well associate an index i of the lattice to each index α , for example, considering the maximum of $|\psi_{\alpha}(i)|^2$.

In the presence of interactions, however, the basic idea behind the LIOMs scheme is to find a unitary transformation U that defines a similar complete set of independent pseudospin-1/2 operators:

$$\tau_i^z = U \sigma_i^z U^\dagger. \quad (6)$$

With the above considerations, the following properties are fulfilled by the τ_i^z operators [12]:

(i) τ_i^z 's are quasilocal operators, in the sense that

$$||[\tau_i^z, \sigma_j^a]|| < ce^{-|i-j|/\xi}, \quad (7)$$

for $a = +, -, z$, and some ξ, c .

(ii) τ_i^z are exactly conserved operators and commute with each other: $[H, \tau_i^z] = 0$ and $[\tau_i^z, \tau_j^z] = 0$.

(iii) τ_i^z have eigenvalues ± 1 ($(\tau_i^z)^2 = 1$) and each subspace has exactly dimension 2^{L-1} .

The unitary U is a composition of local unitary transformations as described by Refs. [35,36]. With the same unitary transformation, one can also define τ_i^\pm , which completes the Pauli algebra. Once the operators τ_i^z has been determined, one can use it to write the Hamiltonian H as a sum of local terms of these interacting LIOMs as

$$H = \sum_i \varepsilon_i \tau_i^z + \sum_{ij} J_{ij} \tau_i^z \tau_j^z + \sum_{ijk} J_{ijk} \tau_i^z \tau_j^z \tau_k^z + \dots, \quad (8)$$

where the couplings between clusters of pseudospins J_{i_1, \dots, i_a} are local in the sense that they decay exponentially as a function of any couple of indices.

It is obvious that each arbitrary arrangement of the eigenvectors of Hamiltonian H in the unitary matrix U of Eq. (6) results in a new set of τ_i operators which satisfy the above-mentioned properties (ii) and (iii) by default. However, we are interested in finding a complete set of τ_i operators that also fulfills the quasilocal requirement which is defined in Eq. (7). Therefore, our goal is to identify a specific arrangement of the eigenstates in U that best fulfill properties (i)–(iii) altogether.

For all choices of W and Δ , total magnetization is a conserved quantity which implies the conservation of the z component of the total spin, $[S^z, H] = 0$ with $S_i^z = \sum_{i=1}^L S_i^z$. Therefore, it defines a good quantum number and we can consider different magnetization sectors separately. Throughout the paper, we use the standard notation $|n\rangle \equiv |S_1^z, S_2^z, \dots, S_L^z\rangle$ with $S_i^z = \uparrow, \downarrow$ for the basis states in real space. In this notation, n in $|n\rangle$ is a decimal integer can be obtained from the L -bit binary representation $|n_1 n_2 \dots n_L\rangle$ as $n = \sum_{i=1}^L n_i 2^{i-1}$, where $n_i = 0, 1$ stands for $S_i^z = \downarrow, \uparrow$ respectively. Using these basis states, we consider an initial set of the basis vectors $\{|n\rangle\}$ in such a way that the Hamiltonian H is block diagonalized and each block corresponds to a subspace with a fixed magnetization. Here we are interested to introduce an efficient way of ordering the LIOM basis states. We use the idea of Ref. [14], which considers a one-to-one mapping between initial basis states $|n\rangle$ and the eigenstates of the system and develop our own scheme to introduce a systematic way of performing such a mapping process. Therefore, we will use the same labeling scheme in which each LIOM basis state can be shown by a binary spectrum as $|\tilde{n}\rangle \equiv |\tau_1^z, \tau_2^z, \dots, \tau_L^z\rangle$ with effective pseudospin $\tau_i^z = \tilde{\downarrow}, \tilde{\uparrow}$. Again, it is convenient to obtain the corresponding integer \tilde{n} for each LIOM basis vector from its binary representation as before. In what follows, we introduce an optimal ordered set of basis states that makes the unitary operator

$$U = \sum_n |\tilde{n}\rangle \langle n| \quad (9)$$

and can be used in Eq. (6) to form a complete set of LIOMs with our desired properties (i)–(iii).

We begin to construct our own approach by considering the noninteracting case, ($\Delta = 0$). In this case, as we already mentioned, LIOMs can be characterized by conserved occupations of single-particle eigenstates and, hence, only the first term on the right-hand side remains in Eq. (8). We start with the reference state $|0\rangle$ with all spins down as the only possible state in its magnetization sector which is also an eigenstate of the system. Therefore, it has a similar representation on both the original and LIOM basis, i.e., $|\underbrace{\downarrow \downarrow \dots \downarrow}_L\rangle = |\underbrace{\downarrow \downarrow \dots \downarrow}_L\rangle$.

By flipping one spin in $|0\rangle$, we get a new state with $S_i^z = L/2 - 1$ and since we have L places for this spin, we have L states in this sector. These states, which are supposed to be ordered according to their binary code, form the original basis states spanning the single-particle block of the Hamiltonian H . After diagonalizing Hamiltonian H , we obtain a set of eigenstates $|\psi_m\rangle$ which needs to be ordered. According to the quasilocal criterion of Eq. (7), we expect an ordered set in which each pseudospin operator τ_i^z is mostly localized around a physical spin operator in real space. Therefore, we can order the obtained eigenstates by determining their maximum overlap with the original basis states. For instance, the first eigenstate is the one that has maximum overlap with the first original basis state. Thus, we need to find the maximum available overlap among the set $\{|\langle \uparrow \underbrace{\downarrow \downarrow \dots \downarrow}_{L-1} |\psi_m\rangle|^2, m =$

$1, \dots, L\}$. If the m_0 th eigenstate is the one with maximum overlap with the first original basis state, it is the first basis state in pseudospin space, which means that $|\uparrow \underbrace{\downarrow \downarrow \dots \downarrow}_{L-1}\rangle = |\psi_{m_0}\rangle$. By

the same token, it is possible to determine the j th eigenstate of this sector by defining the following sequence of eigenstate overlaps for the remaining eigenstates:

$$\{\alpha_m^j = |\langle \downarrow \dots \underbrace{\uparrow}_{j\text{th}} \downarrow |\psi_m\rangle|^2, \\ m = 1, \dots, m_0 - 1, m_0 + 1, \dots, L\}, \quad (10)$$

and finding the eigenstate which maximizes the above overlap and labeling it with $|\downarrow \dots \underbrace{\uparrow}_{j\text{th}} \downarrow\rangle$.

We now proceed to the next sector which has $L(L-1)/2$ basis states with two flipped spins which can be represented by the following notation:

$$|j_1, j_2\rangle = S_{j_1}^+ S_{j_2}^+ |0\rangle = |\downarrow \dots \underbrace{\uparrow}_{j_2\text{th}} \dots \underbrace{\uparrow}_{j_1\text{th}} \dots \downarrow\rangle. \quad (11)$$

The indexes j_1 and j_2 immediately determine the associated integer number n of this basis vector accordingly. Therefore, if we are looking for the \tilde{n} th eigenstate in our optimized set, we should find the one with maximum overlap with its corresponding basis vector. That is, finding the maximum value among the following set of overlaps:

$$\{|\langle j_1, j_2 | \psi_m \rangle|^2, m = 1, \dots, L(L-1)/2\}, \quad (12)$$

and label it as \tilde{n} . The same analysis can be performed in higher-excitation sectors to arrange the final ordered set of the eigenstates properly.

Besides its ease of use and implementation, the main advantage of the above-mentioned algorithm is that it can be generalized even for the case of an interacting system ($\Delta \neq 0$). At the same time, it provides an opportunity to consider the whole Hamiltonian in the full Hilbert-space of the system simultaneously. This is because each eigenstate has only nonzero amplitudes on the basis states of its own sector and hence, in our scheme there is a one-to-one mapping between initial basis states and their corresponding eigenstates of the same sector which prevents sector mixing. Consequently, if the initial basis states are chosen in such a way that the Hamiltonian is block diagonal, the resulting unitary matrix U of the eigenstates obtained after performing our ordering procedure is also block-diagonal. In the remainder of this subsection, we elaborate on the implementation of the algorithm which allows ordering a generic set of energy eigenstates of the system in such a way that the resulting LIOMs satisfy our desired properties (i)–(iii).

Suppose that we have an initial set of the basis vectors $|n\rangle$ in which our Hamiltonian matrix is block diagonal. We can diagonalize this Hamiltonian and obtain the set of energy eigenbasis which is an arbitrary (but fixed) arrangement of energy eigenbasis of the system. Our aim is to rearrange them by assigning a decimal integer that determines their index in our final optimum set. Doing so, we use the fact that each eigenstate of the system is a 2^L component vector which can be expanded based on the Hilbert-space original basis vectors $|n\rangle$ as $|\psi_i\rangle = \sum_{n'=1}^{2^L} A_{n'}^i |n'\rangle$. We can label a given eigenbasis $|\psi_i\rangle$ by integer number n if this eigenstate has the largest absolute amplitude on $|n\rangle$ among all the eigenstates of the system. This means that one needs only to find the index n in such a way that $|A_n^i|^2$ is the largest value of the set $\{|A_n^i|^2, i = 1, \dots, 2^L\}$. In other words, if we consider matrix U , which initially contains the eigenbasis of the Hamiltonian in its columns with an arbitrary arrangement, to find the n th eigenstate in our desired order, we need just to look at the n th row of U and determine which column has the maximum absolute value in this row. This procedure is represented graphically in Fig. 1. The repeated execution of this procedure results in our optimal arrangement of the eigenstates which can optimally satisfy our desired conditions. The procedure outlined above is accurate in the sense that the resulting LIOMs are exactly conserved operators and it is fast because it requires less computational effort as compared to other schemes [22–24] that are based on exact diagonalization. The reason is that in our method, unlike in the above-mentioned schemes, we no longer need to evaluate the expectation values of physical spin operators (L operations) for each energy eigenstate to determine its order in our desired set of eigenstates in U . This will reduce the computational cost associated with rearranging all the eigenstates in U by a factor of ($L \times$ the number of eigenstates) totally. Consequently, since the procedure outlined above does not essentially require the strong disorder limit and, on the other hand, is very simple and fast, and we can use it to obtain our optimum and complete set of LIOMs rapidly and study some structural properties of the system across the phase transition.

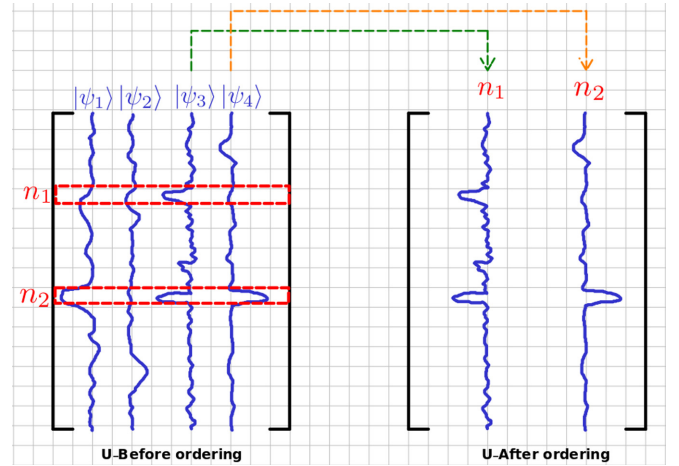


FIG. 1. Graphical representation of the procedure outlined in Sec. II B to arrange the eigenstates of the system in the unitary matrix U which is obtained after diagonalization. The left side shows the matrix of eigenvectors obtained via the exact diagonalization procedure in which usually the eigenstates are ordered according to their corresponding eigenvalues. The right side is the matrix of eigenstates after rearranging them using our algorithm.

III. RESULTS

To examine our method, we have carried out numerical calculations based on the exact diagonalization technique. In what follows, we consider a spin chain with L spins and open boundary conditions. To gain a deeper understanding of the role of interaction in the MBL case, we consider our model in both interacting ($\Delta = 1$) and noninteracting ($\Delta = 0$) regimes, and depending on the system size L , 10^5 to 5×10^3 disorder realizations are employed to obtain the statistics.

A. Effective characterization of LIOM locality

In this section, we demonstrate the quasilocality of the resulting LIOM operators obtained by our algorithm. To this end, we use the two-point correlator between a LIOM operator τ_j^z and physical spin σ_k which is expected [17,18,23] to decay exponentially with distance $|k - j|$ as

$$\langle \tau_j^z \sigma_k^z \rangle = \text{Tr}(\tau_j^z \sigma_k^z) \sim \exp(-|k - j|/\zeta), \quad (13)$$

when j and k are far apart in the MBL regime. In Eq. (13), ζ defines a length scale over which the corresponding LIOM operators are localized. This length scale is related to the spatial correlation length of the eigenstate amplitudes on the Fock space [37,38] and expected to diverge at the critical point.

Figure 2(a) shows the behavior of the logarithm of two-point correlator $\langle \tau_j^z \sigma_k^z \rangle$ versus $|j - k|$ for the LIOM operator which is located near the center of chain in the presence of interaction, $\Delta = 1$. It is obvious that in the deep localized regime ($W \geq 5$), the LIOM operators τ_j^z are strongly localized, and the $\langle \tau_j^z \sigma_k^z \rangle$ profile is mostly localized near the origin j with a fast decaying function to the neighborhood. This is in contrast to the delocalized regime ($W \leq 2.5$) in which such a fast decaying part is obviously absent. Furthermore, there is a clear size dependency, especially near the origin

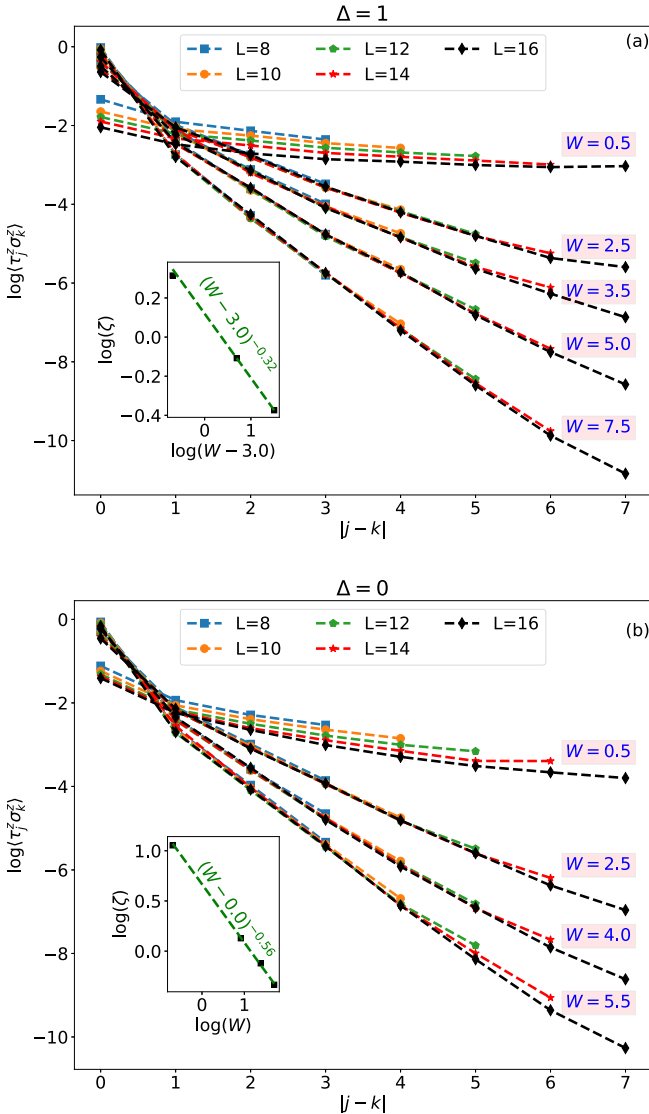


FIG. 2. Decay of two-point correlator $[\log(\langle \tau_j^z \sigma_k^z \rangle)]$ for the LIOM operators localized near the chain center versus $|j - k|$ for different system sizes $L = 8 - 16$ and disorder intensities in both (a) interacting ($\Delta = 1$) and (b) noninteracting ($\Delta = 0$) regimes. Insets show the divergence of length scale ζ as a function of $(W - W_c)$ in the presence and absence of interaction, respectively

which is the characteristic feature of ergodic regime. To make a comparison with noninteracting system ($\Delta = 0$), we have shown the behavior of the $\langle \tau_j^z \sigma_k^z \rangle$ profile for this regime in Fig. 2(b). In this case ($\Delta = 0$), even for very small disorder strength $W = 0.5$ the faster decaying behavior as well as weaker size dependency can be observed in comparison to the MBL counterpart ($\Delta = 1$).

It is also worth mentioning that the characteristic length scale ζ can be extracted from the linear part of the $\log(\langle \tau_j^z \sigma_k^z \rangle)$ versus $|j - k|$ for the largest system size to observe its divergence near the transition point. The inset shows the power-law divergence of the ζ as a function of $(W - W_c)$ on approaching the transition point ($W_c = 3.0$ and $W_c = 0.0$ in the presence and absence of interaction, respectively) in the localized regime ($W > W_c$).

Although the above comparison between the locality of LIOMs in both interacting and noninteracting systems is a piece of qualitative evidence for their difference in the sense of critical disorder needed for localization transition, we will elaborate on this more quantitatively in the coming sections and discuss the critical disorder W_c on which the transition takes place in detail.

B. Percolation transition in connected clusters associated with LIOMs in the Hilbert space

In this section, we introduce a classical percolation problem associated with clusters of LIOMs in the Hilbert space. Indeed, LIOMs are dressed versions of spin operators as given by Eq. (6) and can be viewed as a matrix with elements $(\tau_i^z)_{mn}$ (m and n refer to the row index and column index of this matrix, respectively) in the basis of product states in the S_z basis. Our idea is to interpret this matrix as an adjacency matrix representation of a finite directed graph in which the off-diagonal matrix elements of a given LIOM operator express whether two nodes (basis) are adjacent or not. According to the above discussion, we can write the adjacency matrix like the following:

$$C_{mn} = \begin{cases} 1, & \text{if } |(\tau_i^z)_{mn}| > \eta_c \\ 0, & \text{otherwise.} \end{cases} \quad (14)$$

Here, η_c is a connectivity threshold for deciding below which edge between a pair of basis states on the Hilbert-space graph will be removed or not. It is obvious that if $\eta_c = 0$, we always have a single connected cluster that contains all basis states of the Hilbert space. Therefore, we need to take a nonzero connectivity threshold, $\eta_c > 0$, for the rest of our analysis, which we will describe how to do in the following.

One detail should be described before discussing the estimation procedure. The point is to restrict our numerical calculations to the largest subspace with zero total spin, because the size of the Hilbert space grows exponentially and total magnetization is a conserved quantity in our system. This subspace contains $N_H = \binom{L}{\frac{L}{2}}$ states (nodes). Thus, one naturally expects to have only a single connected cluster with size (number of nodes) N_H for a very weak disorder intensity, namely, $0 < W \ll 1$. This criterion will give us an upper bound for the parameter η_c . In our computation below, we take the maximum possible value for η_c according to its upper bound. Figure 3 shows a typical LIOM operator (represented as a matrix) and its adjacent Hilbert-space graph which is obtained with $\eta_c = 0.05$ for a spin chain with $L = 10$ spins for two random realizations of disorder with disorder strengths $W = 2, 6$ in the MBL regime ($\Delta = 1$).

1. Cluster-size analysis

In the theory of lattice percolation, the emergence of a spanning cluster at the percolation threshold which connects two opposite boundaries on the lattice is a measure of percolation transition [39]. It is obvious that such a definition doesn't really make sense for our considered network here. Therefore, in this subsection, we characterize the percolation transition by analyzing the size of the largest and second-largest connected cluster [40] associated with LIOMs in the

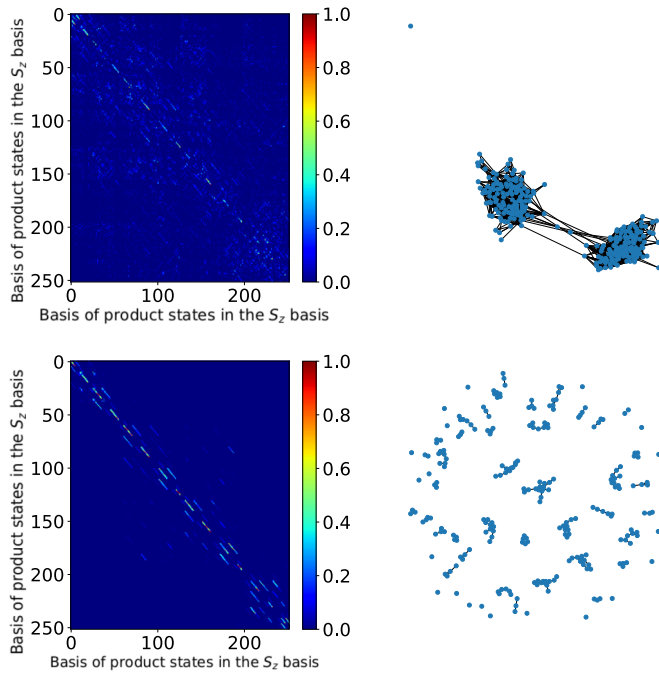


FIG. 3. The left side shows the graphical representation of matrix elements of a typical LIOM operator obtained using Eq. (6) and the ordered set of eigenvectors in unitary matrix U . The right side is the corresponding adjacent graph of the same LIOM operator in the basis of product states in the S_z basis for a spin chain with length $L = 10$ spins for two different disorder intensities $W = 2$ (upper panel) and $W = 6$ (lower panel) in the MBL regime ($\Delta = 1$).

Hilbert space. Starting from the low disorder limit, $W \ll 1$, we expect to have only a single connected cluster with size $S_1 = N_H$ which contains all the nodes of Hilbert space. Due to the localization of eigenstates, one expects to observe a decrease in the largest cluster size by increasing the disorder intensity which means that it only contains a finite fraction of Hilbert-space nodes. In the percolation language, this is equivalent to the formation of smaller size clusters in the network.

We start to illustrate our percolation scenario by calculating the fraction of the largest cluster, defined as the relative size of the largest connected cluster with respect to the Hilbert-space dimension, S_1/N_H . Figure 4 shows how the mean largest cluster size which is averaged over different realizations of disorder decreases as a function of disorder intensity W for a spin chain of length $L = 16$. Additionally, we can also compute the average size of the second-largest cluster S_2 to confirm the transition threshold. This is because, on finite systems, the size of the largest cluster grows by adding smaller clusters, and therefore it is possible to determine the vicinity of the transition point by locating the point where the second-largest cluster size reaches its maximum. The peak position coincides with the percolation threshold in the thermodynamic limit [40]. We observe that the normalized size of the second-largest cluster, S_2/S_2^{\max} , also peaks near the percolation transition. We have plotted the same quantities for both noninteracting and interacting regimes in Figs. 4(a) and 4(b), respectively, to make a comparison possible. It is obvious that the presence of interaction shifts the percolation

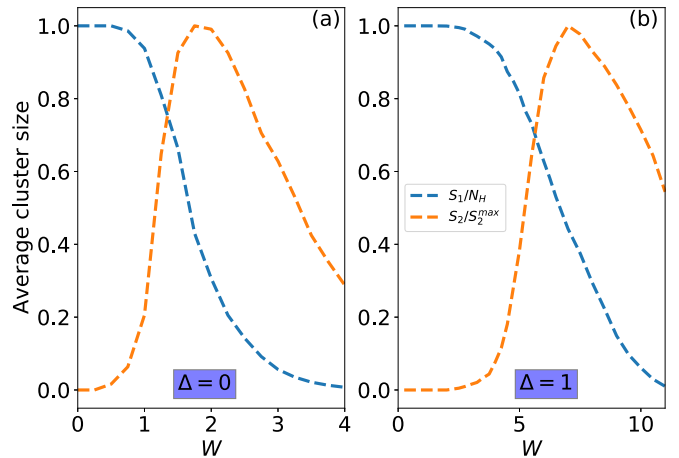


FIG. 4. Behavior of the average largest and second-largest cluster sizes versus disorder intensity W for a spin chain with $L = 16$ spins in both (a) the noninteracting ($\Delta = 0$) and (b) interacting ($\Delta = 1$) regimes. It is obvious one needs a stronger disorder to reach the nonpercolating regime in the presence of interaction.

threshold W_c toward the stronger intensity of disorder, however, we leave the discussion of more accurate determination of such a percolation threshold for the sections that follow.

2. Universal feature and finite-size scaling analysis near the transition point

The more precise determination of the percolation threshold for the adjacent graph of the LIOMs can be obtained using scaling analysis. Following the arguments of Ref. [29], we first focus our attention on the scaling of the mean cluster size, and since the largest cluster is not essentially a typical one, we take the cluster C that contains the basis state of corresponding eigenstate $|\psi_0\rangle$ with the closest energy to the mean value of the energy spectrum and compute the geometric average of its size over different realizations of disorder as

$$S_{\text{typ}} = \exp\left(\frac{1}{N_r} \sum_r \ln(s_r)\right). \quad (15)$$

Here, s_r is the number of nodes (eigenstates) in the cluster C for a given realization r of disorder and N_r is the number of disorder realizations. According to the finite-size scaling [39], the scaling of the normalized cluster sizes near the transition point can be stated as [29]

$$S_{\text{typ}}/N_H \sim f((W - W_c)L^{\frac{1}{\nu}}), \quad (16)$$

in which the exponent ν is called the correlation length exponent. Therefore, by performing data collapse analysis, it is possible to obtain the percolation threshold W_c and critical exponent ν . The results of such data collapse, yielding the critical exponent $\nu(\Delta = 1) = 2.0$ and $\nu(\Delta = 0) = 2.5$ in the presence and absence of interaction is shown in Figs. 5(a) and 5(b), respectively. We should emphasize that in the data collapse procedure in the noninteracting regime $\Delta = 0$, we constrained the critical point $W_c = 0.0$ as a transition point of the corresponding XX model [41]. We note that the resulting exponent ν satisfies the Harris-CCFS bound ($\nu \geq \frac{2}{d}$)

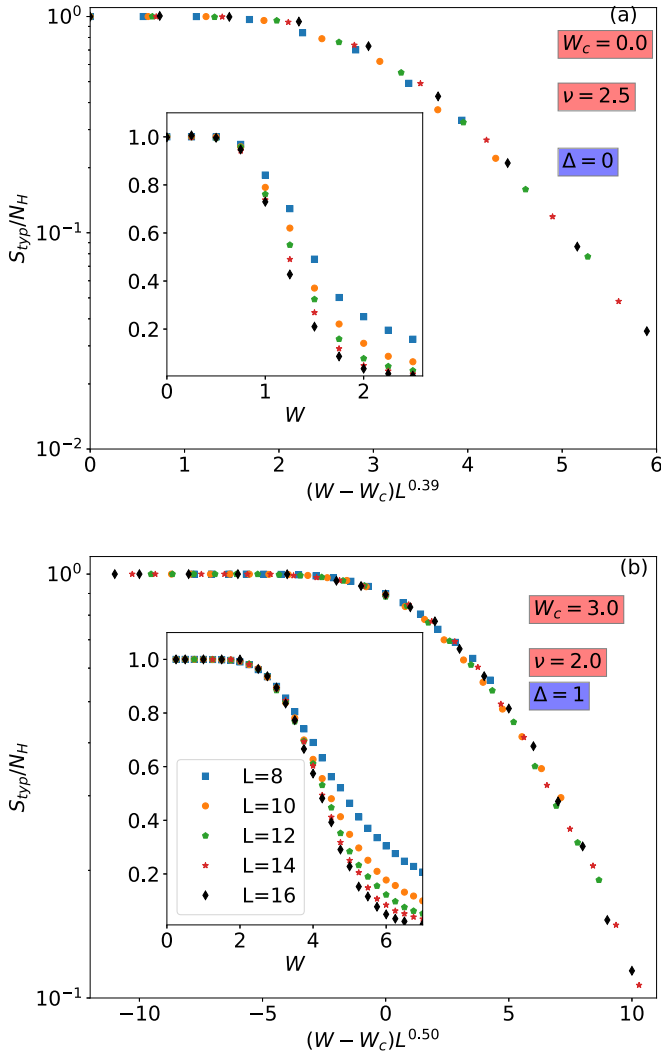


FIG. 5. The resulting data collapse of S_{typ}/N_H onto a scaling function of $(W - W_c)L^{1/\nu}$ which is obtained for spin chains with different lengths ($L = 8 - 16$) both in the (a) absence $\Delta = 0$ and (b) presence $\Delta = 1$ of interaction in the localized phase. The critical parameters $W_c = 3.0, 0.0$, and $\nu = 2.0, 2.5$ is obtained for the case of MBL and Anderson transition, respectively. Insets show the corresponding raw data.

[42,43], confirmed for the ergodic to MBL transition recently [29,44,45].

In addition, the percolation threshold is quite different as $W_c = 3.0$ and $W_c = 0.0$ for the case of the interacting and noninteracting systems, respectively. It is worth mentioning that beyond the error of our analysis, the percolation threshold for the case of the interacting system coincides with the ergodic to MBL transition point $W_c \approx 3.5$ [33], which shows that our system experiences a percolation transition in its corresponding LIOMs across the MBL transition.

Before ending this subsection, let us shed more light on the effect of changing the estimated parameter η_c in our clusterization mechanism. As we already discussed, we set the value of this parameter by the largest value of η_c for which the size of the largest cluster is exactly equal to the Hilbert-space dimension N_H . It is certainly possible to consider smaller

nonzero values for the connectivity threshold parameter (any value in $(0, \eta_c]$). However, our investigations showed that the changing of η_c may change a bit the percolation threshold W_c , but the correlation length exponent ν will not change.

C. Distribution of local observables on the clusters

The last quantity which we are interested in is the distribution of the eigenstate expectation values of local observables which are shown to vary significantly across the MBL transition [46,47]. In doing so, let us consider cluster C , which contains the eigenstate $|\psi_0\rangle$ with size s , as we discussed before, and define the following quantity for the cluster [29]:

$$m_l = \frac{1}{s} \sum'_n \langle n | \tau_l^z | n \rangle, \quad (17)$$

where \sum' denotes the restrictions imposed by considering only the eigenstates in C in summation. This is indeed the average local magnetization of the cluster and can be obtained by averaging only over the diagonal entries of the corresponding LIOM operator which belongs to the cluster C . We are interested in the distribution of this quantity which is averaged over different realizations of disorder.

Before going further, let us point out the meaning of the diagonal element of τ_l^z using Eqs. (6) and (9),

$$\langle n | \tau_l^z | n \rangle = \sum_m (\sigma_l^z)_{mm} |\psi_m(n)|^2, \quad (18)$$

where $\psi_m(n)$ represents the amplitude of the m th eigenstate on the n th basis state and $(\sigma_l^z)_{mm}$ is the m th element of diagonal matrix σ_l^z with entries $+1$ or -1 . Now, the average local magnetization of cluster C defined in Eq. (17) can be expressed as

$$m_l = \frac{1}{s} \sum'_n \sum_m (\sigma_l^z)_{mm} |\psi_m(n)|^2. \quad (19)$$

Figure 6 shows the distribution of this quantity for the largest system size $L = 16$ spins in both MBL and Anderson regimes. In the case of interacting regime $\Delta = 1$ for weak disorder intensity $W = 0.5$, we have a single peak around zero. This is because in the ergodic phase, cluster C contains all the basis states of the Hilbert space and, hence, $\sum'_n \rightarrow \sum_{n=1}^{N_H}$ and $s = N_H$. Therefore, it is convenient to perform the summation over n first and use the normalization condition of the eigenstates, $\sum_n |\psi_m(n)|^2 = 1$, which results in $m_l = \text{Tr}(\sigma_l^z) = 0$. This is the reason for observing a single peak at $m_l = 0$ in the distribution function $P(m_l)$ in Fig. 6 for weak disorder regime ($W = 0.5$ and $\Delta = 1$).

By increasing the disorder intensity W , since the size of cluster C starts to deviate (decreases) from the size of Hilbert space, some of the nodes (basis states) will be excluded from the summation over n in Eq. (19). Consequently, it is the eigenstate profile $\psi_m(n)$ in Eq. (19) which plays a crucial role in characterizing the distribution function $P(m_l)$ and one needs to know its exact form to describe the smooth part of $P(m_l)$ in the intermediate regime $W_c < W < \infty$. For the case of very strong disorder limit ($W \rightarrow \infty$), the probability of having only a single node in cluster C increases, which yields $\psi_m(n) \sim \delta_{m,n}$ and $s = 1$ and hence $m_l = \pm 1$. So one

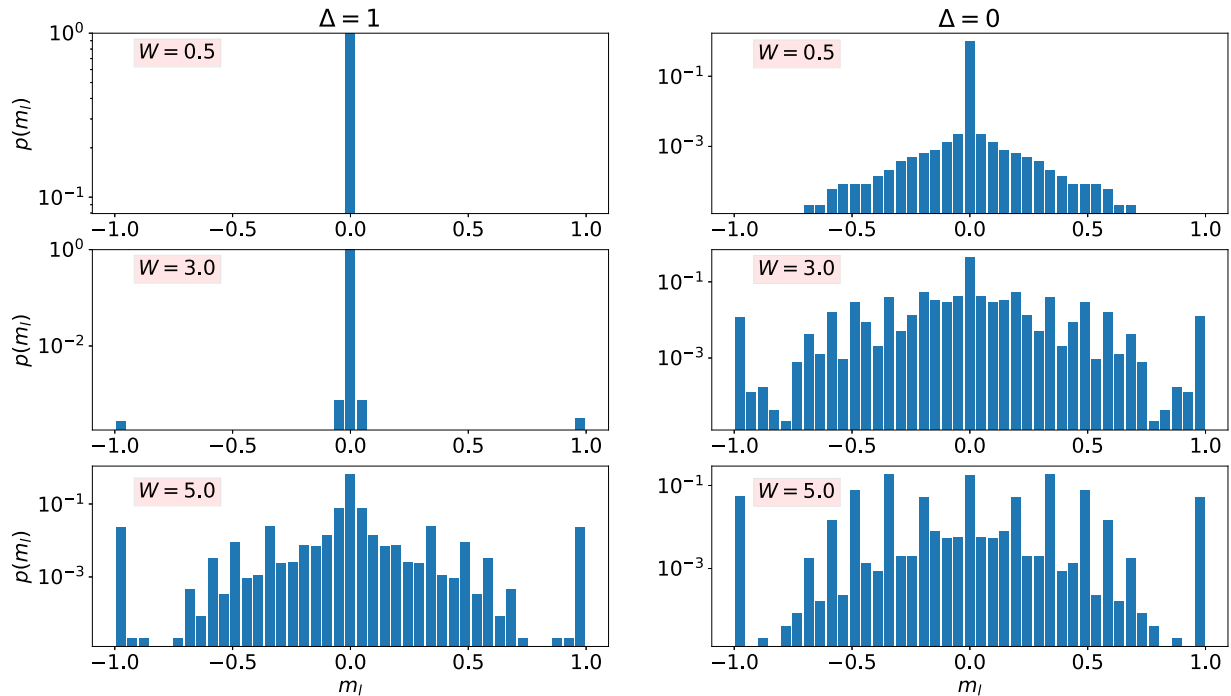


FIG. 6. Distribution function $P(m_l)$ of the average local magnetization of cluster m_l , which is the average expectation values of LIOM operator τ_i^z over the nodes of this cluster both for $\Delta = 0$ and $\Delta = 1$.

naturally expects to observe two single peaks at $m_l = \pm 1$ for the distribution function $P(m_l)$ in this regime. The plots in Fig. 6 show that the existence of such single-node clusters is much more probable even for very small disorder intensities in the case of the noninteracting regime ($\Delta = 0$).

IV. CONCLUDING REMARKS

We provided a fast and accurate method to efficiently obtain LIOMs for a disordered system that undergoes MBL transition. We showed that an optimized set of eigenvectors obtained by locating their maximum overlap with Hilbert-space basis can be used to obtain the desired set of LIOM operators. We showed that the resulting LIOMs experience a percolation transition in their graph representation in Hilbert space by increasing disorder intensity. We also compared the

critical disorder and critical exponent describing percolation transition for both interacting (MBL) and noninteracting (Anderson) regimes. Our analysis showed that there is a concrete connection between the ergodic to MBL transition and the structural properties of LIOMs in their graph representation on the Hilbert space.

ACKNOWLEDGMENTS

We are extremely grateful to A. Scardicchio for multiple illuminated discussions, insights, and guidance to improve our work. We acknowledge the CINECA award under the ISCRA initiative for the availability of high performance computing resources and support. M.A. acknowledges the support of the Abdus Salam (ICTP) associateship program.

-
- [1] K. Agarwal, S. Gopalakrishnan, M. Knap, M. Müller, and E. Demler, Anomalous Diffusion and Griffiths Effects Near the Many-Body Localization Transition, *Phys. Rev. Lett.* **114**, 160401 (2015).
- [2] I. V. Gornyi, A. D. Mirlin, and D. G. Polyakov, Interacting Electrons in Disordered Wires: Anderson Localization and Low- T Transport, *Phys. Rev. Lett.* **95**, 206603 (2005).
- [3] D. M. Basko, I. L. Aleiner, and B. L. Altshuler, Metal-insulator transition in a weakly interacting many-electron system with localized single-particle states, *Ann. Phys.* **321**, 1126 (2006).
- [4] M. Žnidarič, A. Scardicchio, and V. K. Varma, Diffusive and Subdiffusive Spin Transport in the Ergodic Phase of a Many-Body Localizable System, *Phys. Rev. Lett.* **117**, 040601 (2016).
- [5] R. K. Panda, A. Scardicchio, M. Schulz, S. R. Taylor, M. Znidarič, Can we study the many-body localisation transition, *Europhys. Lett.* **128**, 67003 (2020).
- [6] M. Schulz, S. R. Taylor, C. A. Hooley, A. Scardicchio, Energy transport in a disordered spin chain with broken $U(1)$ symmetry: Diffusion, subdiffusion, and many-body localization, *Phys. Rev. B* **98**, 180201(R) (2018).
- [7] V. Oganesyan and D. A. Huse, Localization of interacting fermions at high temperature, *Phys. Rev. B* **75**, 155111 (2007).
- [8] M. Žnidarič, T. Prosen, and P. Prelovšek, Many-body localization in the Heisenberg XXZ magnet in a random field, *Phys. Rev. B* **77**, 064426 (2008).

- [9] J. H. Bardarson, F. Pollmann, and J. E. Moore, Unbounded Growth of Entanglement in Models of Many-Body Localization, *Phys. Rev. Lett.* **109**, 017202 (2012).
- [10] S. Gopalakrishnan, M. Müller, V. Khemani, M. Knap, E. Demler, and D. A. Huse, Low-frequency conductivity in many-body localized systems, *Phys. Rev. B* **92**, 104202 (2015).
- [11] A. De Luca and A. Scardicchio, Ergodicity breaking in a model showing many-body localization, *Europhys. Lett.* **101**, 37003 (2013).
- [12] V. Ros, M. Müller, and A. Scardicchio, Integrals of motion in the many-body localized phase, *Nucl. Phys. B* **891**, 420 (2015).
- [13] M. Serbyn, Z. Papić, and D. A. Abanin, Local Conservation Laws and the Structure of the Many-Body Localized States, *Phys. Rev. Lett.* **111**, 127201 (2013).
- [14] D. A. Huse, R. Nandkishore, and V. Oganesyan, Phenomenology of fully many-body-localized systems, *Phys. Rev. B* **90**, 174202 (2014).
- [15] P. W. Anderson, Absence of diffusion in certain random lattices, *Phys. Rev.* **109**, 1492 (1958).
- [16] J. Z. Imbrie, Diagonalization and Many-Body Localization for a Disordered Quantum Spin Chain, *Phys. Rev. Lett.* **117**, 027201 (2016).
- [17] A. Chandran, I. H. Kim, G. Vidal, and D. A. Abanin, Diagonalization and Many-Body Localization for a Disordered Quantum Spin Chain, *Phys. Rev. B* **91**, 085425 (2015).
- [18] S. D. Geraedts, R. N. Bhatt, and R. Nandkishore, Emergent local integrals of motion without a complete set of localized eigenstates, *Phys. Rev. B* **95**, 064204 (2017).
- [19] S. Inglis and L. Pollet, Accessing Many-Body Localized States through the Generalized Gibbs Ensemble, *Phys. Rev. Lett.* **117**, 120402 (2016).
- [20] L. Rademaker and M. Ortuño, Explicit Local Integrals of Motion for the Many-Body Localized State, *Phys. Rev. Lett.* **116**, 010404 (2016).
- [21] T. E. O'Brien, D. A. Abanin, G. Vidal, and Z. Papić, Explicit construction of local conserved operators in disordered many-body systems, *Phys. Rev. B* **94**, 144208 (2016).
- [22] M. Goihl, M. Gluza, C. Krumnow, and J. Eisert, Construction of exact constants of motion and effective models for many-body localized systems, *Phys. Rev. B* **97**, 134202 (2018).
- [23] P. Peng, Z. Li, H. Yan, K. X. Wei, and P. Cappellaro, Comparing many-body localization lengths via nonperturbative construction of local integrals of motion, *Phys. Rev. B* **100**, 214203 (2019).
- [24] A. Chandran, J. Carrasquilla, I. H. Kim, D. A. Abanin, and G. Vidal, Spectral tensor networks for many-body localization, *Phys. Rev. B* **92**, 024201 (2015).
- [25] D. Pekker and B. K. Clark, Encoding the structure of many-body localization with matrix product operators, *Phys. Rev. B* **95**, 035116 (2017).
- [26] F. Pollmann, V. Khemani, J. I. Cirac, and S. L. Sondhi, Efficient variational diagonalization of fully many-body localized Hamiltonians, *Phys. Rev. B* **94**, 041116 (2016).
- [27] T. B. Wahl, A. Pal, and S. H. Simon, Efficient Representation of Fully Many-Body Localized Systems using Tensor Networks, *Phys. Rev. X* **7**, 021018 (2017).
- [28] L. Rademaker, M. Ortuño, and A. M. Somoza, Many-body localization from the perspective of Integrals of Motion, *Ann. Phys.* **529**, 1600322 (2017).
- [29] S. Roy, J. T. Chalker, and D. E. Logan, Percolation in Fock space as a proxy for many-body localization, *Phys. Rev. B* **99**, 104206 (2019).
- [30] S. Roy, D. E. Logan, and J. T. Chalker, Exact solution of a percolation analog for the many-body localization transition, *Phys. Rev. B* **99**, 220201(R) (2019).
- [31] P. Prelovšek, M. Mierzejewski, J. Kršnik, and O. S. Barisic, Many-body localization as a percolation phenomenon, *Phys. Rev. B* **103**, 045139 (2021).
- [32] A. Pal and D. A. Huse, Many-body localization phase transition, *Phys. Rev. B* **82**, 174411 (2010).
- [33] D. J. Luitz, N. Laflorencie, and F. Alet, Many-body localization edge in the random-field Heisenberg chain, *Phys. Rev. B* **91**, 081103(R) (2015).
- [34] P. Jordan and E. Wigner, About the Pauli exclusion principle, *Z. Phys.* **47**, 631 (1928).
- [35] J. Z. Imbrie, On many-body localization for quantum spin chains, *J. Stat. Phys.* **163**, 998 (2016).
- [36] J. Z. Imbrie, V. Ros, and A. Scardicchio, Local integrals of motion in many-body localized systems, *Ann. Phys.* **529**, 1600278 (2017).
- [37] G. De Tomasi, I. M. Khaymovich, F. Pollmann, and S. Warzel, Rare thermal bubbles at the many-body localization transition from the Fock space point of view, *Phys. Rev. B* **104**, 024202 (2021).
- [38] S. Roy and D. E. Logan, Fock-space anatomy of eigenstates across the many-body localization transition, *Phys. Rev. B* **104**, 174201 (2021).
- [39] Percolation I, in *Fractals and Disordered Systems*, edited by A. Bunde and S. Havlin (Springer, Berlin, Heidelberg, 1991), pp. 51–96.
- [40] A. Margolina, H. J. Herrmann, and D. Stauffer, Size of largest and second largest cluster in random percolation, *Phys. Lett. A* **93**, 73 (1982).
- [41] T. Devakul, V. Khemani, F. Pollmann, D. A. Huse, and S. L. Sondhi, Obtaining highly excited eigenstates of the localized XX chain via DMRG-X, *Phil. Trans. R. Soc. A* **375**, 20160431 (2017).
- [42] A. B. Harris, Effect of random defects on the critical behaviour of Ising models, *J. Phys. C: Solid State Phys.* **7**, 1671 (1974).
- [43] J. T. Chayes, L. Chayes, D. S. Fisher, and T. Spencer, Finite-Size Scaling and Correlation Lengths for Disordered Systems, *Phys. Rev. Lett.* **57**, 2999 (1986).
- [44] A. Chandran, C. R. Laumann, and V. Oganesyan, Finite size scaling bounds on many-body localized phase transitions, [arXiv:1509.04285](https://arxiv.org/abs/1509.04285).
- [45] P. Sierant, M. Lewenstein, A. Scardicchio, and J. Zakrzewski, Stability of many-body localization in kicked Ising model, [arXiv:2203.15697](https://arxiv.org/abs/2203.15697).
- [46] C. L. Baldwin, C. R. Laumann, A. Pal, and A. Scardicchio, The many-body localized phase of the quantum random energy model, *Phys. Rev. B* **93**, 024202 (2016).
- [47] D. J. Luitz, Long tail distributions near the many-body localization transition, *Phys. Rev. B* **93**, 134201 (2016).